HAL
open science

Advancements in Gd-based neutron detection: $\gamma - \gamma$ coincidence approach

Jonathan Dumazert, Romain Coulon, Gwenole Corre, Matthieu Hamel, Quentin Lecomte, Vladimir Kondrasovs, Chrystèle Dehé-Pittance, Guillaume Bertrand, Jean-Michel Bourbotte, Sara Garti, et al.

To cite this version:

Jonathan Dumazert, Romain Coulon, Gwenole Corre, Matthieu Hamel, Quentin Lecomte, et al.. Advancements in Gd-based neutron detection: $\gamma - \gamma$ coincidence approach. Nuclear Instruments and Methods in Physics Research Section A: Accelerators, Spectrometers, Detectors and Associated Equipment, 2020, 954, pp.161199. 10.1016/j.nima.2018.09.034 . cea-01916037

HAL Id: cea-01916037

https://cea.hal.science/cea-01916037v1

Submitted on 24 Feb 2022

HAL is a multi-disciplinary open access archive for the deposit and dissemination of scientific research documents, whether they are published or not. The documents may come from teaching and research institutions in France or abroad, or from public or private research centers.

L'archive ouverte pluridisciplinaire **HAL**, est destinée au dépôt et à la diffusion de documents scientifiques de niveau recherche, publiés ou non, émanant des établissements d'enseignement et de recherche français ou étrangers, des laboratoires publics ou privés.

Version of Record: https://www.sciencedirect.com/science/article/pii/S0168900218311781
Manuscript_5062c0e503459a5e4a42e137be7a8bd2

Advancements in Gd-based neutron detection: γ-γ coincidence approach

J. Dumazert*, R. Coulon, G. Corre, M. Hamel, Q. Lecomte, V. Kondrasovs, C. Dehé-Pittance, G. H. V. Bertrand, J.-M. Bourbotte, S. Garti, R. Woo

CEA, LIST, Laboratoire Capteurs Architectures Electroniques, 91191 Gif-sur-Yvette, France.

***Abstract* — CEA LIST is working of the development of a high-sensitivity thermal neutron counter, based on the insertion of gadolinium in spherical plastic scintillators. As the radiation sensor comprises one or several volumes of scintillating polymers, it is, by nature, sensitive to both neutron and gamma radiations. This property allows the development of a versatile detector, provided that it is possible to algorithmically separate the signature of both types of radiations. The technologically building brick is, moreover, to be implemented in a transportable (< 15 kg) system, handled by a first intervention task force in an exposed area. The aim of this paper is to study, both through Monte Carlo simulation and experimentally, an algorithmic architecture of the measurement chain discriminating neutron and gamma events. The presentation is subdivided in three main sections. First, we detail a comparative study between the outputs of a numerical modelling tool, developed to simulate the total response of the sensor to varying radiation sources and the results of a series of experiments carried out in a controlled environment. Second, we describe the building and numerical pre-validation of a simulation code dedicated to the study of consolidated algorithmic architecture, namely *γ-γ quasi-coincidence* on two adjacent plastic scintillators. Third, we comment on an experimental study of γ-γ quasi-coincidence, Gd-based neutron detection and a comparison between the results and the estimated of the numerical study. We conclude with the presentation of first estimates of neutron sensitivity), gamma-background vulnerability, and n/γ discrimination ratio for the scaled and assessed, material and algorithmic architectures.**

***Index Terms* — Neutron counter. Plastic scintillator. Gadolinium. Coincidence filtering.**

I. Introduction

In the frame of the inter-ministerial R&D program on Chemical, Biological, Radiological, Nuclear, and high yield Explosive (CBRNE) countermeasures, French Atomic Energy Commission (CEA LIST) is working of the development of a high-sensitivity thermal neutron counter, based on the insertion of gadolinium (Gd) in spherical plastic scintillators. The concept of the said detector was patented [1] and the first theoretical and experimental studies have shown the deployment potential of the concept, as well as the necessary incremental improvements for the definition of a consolidated technological solution [2]. In the original, modeled, assembled and tested prototype, neutron detection was based on the signature of gamma rays with energy above 5 MeVee, emitted in the radiative cascade following the capture of a thermal neutron by a Gd nucleus. This signature is thus isolated *via* a mere pulse height discrimination (PHD). The estimated neutron sensitivity, of the order of $1\ \mathrm{cps}/(\mathrm{n.cm^{-2}.s^{-1}})$, was found compatible with Special Nuclear Material detection issues. The false count rate evolution, however, highlights a vulnerability to cosmic rays (muons) and high-energy gamma rays (fission), which may severely impact neutron detection limits for medium gamma dose rates (10-100 $\mu\mathrm{Sv.h^{-1}}$).

As the radiation sensor comprises one or several volumes of scintillating polymers, it is, by nature, sensitive to both neutron and gamma radiations. This property allows the development of a versatile detector, provided that it is possible to algorithmically separate the signature of both types of radiations. Contrary to modified plastic scintillators with neutron/gamma (n/γ) discriminating properties [3], such a detection ensemble allows the detection of slow neutron capture events that are not preceded by a proton recoil event. The combination of both sensing bricks should lead to wide-spectrum neutron detection, and ultimately, spectral information on the incident neutron radiation. The technological building brick is, moreover, to be implemented in a transportable (< 15 kg) system, handled by a first intervention task force on an exposed area. The aim of this paper is to study, both through Monte Carlo simulation and experimentally, an algorithmic architecture of the measurement chain discriminating neutron and gamma events.

II. Thermal neutron capture by Gd nuclei and State of the art

In this section, we briefly recall the main characteristics of $^{155}\mathrm{Gd(n,\gamma)}$ and $^{157}\mathrm{Gd(n,\gamma)}$ neutron capture reactions. On the basis of the identification of the reaction products of interest, we establish a state of the art of the various material and algorithmic architectures dedicated to the quantification of this signature. Several architectural designs are then proposed, that are to be studied throughout the course of the program.

© 2018. This manuscript version is made available under the Elsevier user license
https://www.elsevier.com/open-access/userlicense/1.0/

A. *High-energy signature of $^{155}Gd(n,\gamma)$ and $^{157}Gd(n,\gamma)$ neutron capture reactions*

Neutron capture by Gd-155 and Gd-157 results in the isotopic change of the nucleus, with reaction products freed as nuclear and atomic structures rearrange: gamma rays, internal conversion electrons, X rays and Auger electrons [4]. This de-excitation source term, amounting for an average 8048.2 ± 0.6 keV Q-value in natural Gd, is largely dominated by a gamma-ray continuum characterized by a high multiplicity: about 99 % of the Q-value being carried by an average number of 3 to 5 simultaneously-emitted photons [5]. The emission spectrum shows a high-energy signature between 2 and 8 MeV, with several intense gamma rays (6.75 MeV; 7.86 MeV) dominating a continuum. This observation is at the root of the neutron detection strategy we followed, that consists in isolating the signature, inside the plastic sensors, of the high-energy gamma source term released after $\mathrm{Gd(n,\gamma)}$ capture reaction. This signature indeed provides access to favorable n/γ signal-to-noise ratio (SNR) above a 2.6 MeV energy threshold (PHD). The said threshold corresponds to the highest-energy prominent gamma ray (Tl-208) emitted by radionuclides in the disintegration chains of U-238 and Th-232 of natural radioactivity [6]. Now the quantification of a significant fraction of this energetic electromagnetic source term requires a high-density or large-volume sensor, and governs the conception and optimization rules for dedicated detection schemes, whose state of the art is summarily described in the next paragraph.

B. *Reference work on large-volume solid neutron detectors based on the gamma-ray signature of Gd captures*

The previously detailed neutron detection strategy requires the interaction of photons with more than 3 MeV energy. Hence a scale-up of the radiation sensor must be operated according to a tradeoff between cost and detection efficiency. The latter consideration is the reason why liquid-or-plastic-scintillator-based technological solutions tend to be favored. As an illustration, attenuation coefficients for 3-MeV-energy photons [7] show that 50 % absorption yield is expected after 17.5 cm range in plastic.

As far as fieldable detectors are concerned, solid, plastic sensors are preferentially selected as mechanically robust, watertight, and non-fusible. De Vita *et al.* [8] thus introduced a neutron detection scheme based on $\mathrm{Gd(n,\gamma)}$ reactions in which $200 \times 6 \times 6$ cm^3 plastic scintillator (PS) blocks are wrapped in 50-µm Mylar sheets covered with a 25-µm Gd_2O_3 layer. PS blocks act as a neutron moderator the fast, incident fission spectrum, and as a sensor for $\mathrm{Gd(n,\gamma)}$-reaction gamma rays up to 8 MeV. Neutron/gamma discrimination was based on hit multiplicity, *i.e.* on the number of events registered in several isolated bars following neutron or gamma-ray diffusion. GEANT4 simulations showed that, by enforcing a hit multiplicity equal to 3 for n/γ discrimination, a rejection ratio of 145 was accessible while maintaining a theoretical neutron detection efficiency of 28 %. The concept was transposed to Radiation Portal Monitors (RPM), and Fanchini reported [9] a 100-% detection yield in presence of a moderated $2{\cdot}10^5$-n.s^{-1} Cf-252 source a distance of 2.5 m, and a null false alarm rate in presence of a 20-µSv.h^{-1} gamma-ray dose rate (Cs-137).

The development of large-volume PS with heterogeneous Gd-loading was also pursued in the fields of fundamental research and fixed facility instrumentation. Pawełczak *et al.* [10] described a prototype said "Neutron Sandwich Transmuter/Activation-γ Radiator" (NSTAR), whose purpose was to determine the neutron burst multiplicity at the output of D-D fusion neutron generator. NSTAR is formed by a stack of $10 \times 20 \times 2$ cm^3 fast-response PS (BC-408, Saint-Gobain), interlined by 1-mm thick, Gd_2O_3-loaded polydimethylsiloxane foils (resulting heterogeneous mass load of 0.5 wt % (Gd). The module performs n/γ discrimination on the basis of a temporal correlation between the signature of proton recoils, associated with the first diffusions of fast neutrons within the plastic, and the delayed signature of gamma rays released after the capture of the moderated neutron by a Gd-155 or Gd-157 nucleus. By setting a [7-97 µs] correlation gate, and rejecting signals with measured energies above 5 MeV-electron equivalent (MeVee), the authors obtained n/γ SNR between 10^2 and 10^3.

Another noticeable application field relates to the detection of electron antineutrinos *via* neutron emission, following the interaction of said antineutrons proton nuclei in a hydrogenous target. In view of this indirect detection, Huroda *et al.* [11] described a transportable and reconfigurable detector said "Plastic AntiNeutrino Detector Array" (PANDA). The sensor is made of $10 \times 10 \times 100$ cm^3 PS bars, wrapped in Gd-coated Mylar films (surface mass density of 4.9 mg.cm^{-2}), and concatenated to form a several hundred of kilogram target. The volume and granularity of the target allow neutron/background discrimination based on a combination of PHD, event multiplicity and temporal correlation approaches. In this algorithmic architectures, neutrons are detected on the grounds of:

- a temporal correlation between prompt and delayed ($\mathrm{Gd(n,\gamma)}$ capture) events lying within a [6-200 µs] gate;
- a measured delayed energy, integrated over all Gd-coated PS, between entre 3 and 8 MeVee**;**
- additional filters based on first maximal and second maximal energies laid down in separately considered modules.

A 360-kg prototype [12] said PANDA36 was assembled and set at sea level, at a distance of 36 m from the 3.4-GWth reactor of Ohi Power Station (Kansai Electric Power Co., Inc.). Electron antineutrino are indeed produced along the disintegration chains of U-235 and Pu-239, and thus may be used as a signal for surveilling and monitoring nuclear power plants. The expected antineutrino-induced count rate was confirmed experimentally by the authors, at the expense of a complexified discrimination scheme, based on the topology of coincidence events in view of muon rejection.

In order to address the issues of very-high-energy (20 MeV-1 GeV) neutron counting and dosimetry, Roecker *et al.* [13] conceived a 1-ton "Multiplicity and Recoil Spectrometer" (MARS) transportable by hoist. MARS is formed by two mixed PS/Gd $100 \times 75 \times 25$ cm^3 ensembles, each of them constituted of 12-cm-thick PS interlined with Gd-coated Mylar foils. The counting of 20-100 MeV neutrons is based on a capture-gated temporal correlation as described in references [9,10]. To detect higher-

energy neutrons, a 101 × 71 × 20 cm^3 Pb plate is inserted between both PS/Gd ensembles, and acts a nuclear spallation target: very fast neutrons the induce lower-energy neutrons, in the order of 1-2 MeV, with multiplicity depending on incident neutron radiation. Secondary neutrons are subsequently diffused in plastic, and undergo $\mathrm{Gd(n,\gamma)}$ capture reaction within mean delay 19 ± 3 µs. GEANT4 simulations led to an estimation of MARS neutron detection efficiency of 12.8 ± 0.1 %.

C. Algorithmic filtering from neutron/background discrimination

Abovementioned reference work highlights three types of event filtering, dedicated to the discrimination of neutron-induced pulses from gamma-ray and muon background:

- by the measured energy (proportional to the amplitude or area of pulses), above the lower threshold lying between 3 and 5 MeVee, and an upper threshold between 8 and 9 MeVee. This approach is based on the spectral extent of the continuum deprived of the extent of significant natural gamma background;
- by the multiplicity of gamma-ray events detected coincidentally. This approach relies on the multiplicity of gamma emission following reactions, forming a consolidated signature of neutron-induced events. However, this multiple signature requires a separation between both events;
- by the temporal correlation between two pulses within a window typically comprised between 10 and 200 µs. This approach has roots in the fact that some slow neutron captures are preceded by fast neutron diffusion in the PS medium (recoil of a directly ionizing ion).The following of both events therefore constitutes a consolidated signature of the interaction history of one neutron within the detection ensemble. As previously, this method requires the separation of both events, and is only effective when a fast neutron-induced ion recoil is detectable.

The first PHD filter was systematically used in the algorithmic architecture of the detectors. Nonetheless, previous studies [2,8] show that an algorithmic architecture reduced to a sole PHD filter remains vulnerable to background radiations under an elevated gamma-ray dose rate, typically between 20 to 30 µSv.h^{-1}. Thus it appears necessary to enrich the architecture with one or more filters to increase the SNR. The hereby detailed study concerns a filter based on gamma-ray-event temporal coincidence, with the purpose of identifying multiple gamma-ray emissions associated with Gd de-excitations. This study relies on both simulations and laboratory experiments.

III. Study of a Numerical Model for Material Design

The conception and optimization of a material architecture for the detector was carried out by means of the MCNP6.1 code for particle transport [14]. The first step was to verify that valid modelling tools and schemes were available for the delivery of output data, representing real physical processes inside the sensor and useable for the computation of neutron sensitivity and detection limits in a mixed n/γ field. We based the validation study on the total response of the radiation sensor and a PHD detection algorithm to the radioactivity of a lead-shielded, neutron-emitting source (Cf-252). In Monte Carlo simulations, the output corresponds to an energy deposition yield labeled Y (expressed in deposition per disintegration, $\mathrm{d.dis^{-1}}$) between a lower threshold varying between 2 and 4 MeVee and a 9 MeVee upper threshold. This expected response is then to be compared with the experimental count rate R (in count per disintegration, $\mathrm{c.dis^{-1}}$) integrated between the same thresholds.

A. Description of the numerical model and simulated response to Cf-252

We modeled two 10 × 10 × 10 cm^3 PS commercialized by Eljen Technlogy, and referenced EJ-200 [15]. As neutron diffusion strongly depends on molecular organization in dense and hydrogenous media, we used transport data associated with benzene nuclei at 300 °K. Both SP are positioned head-to-tail, and respective labeled S1 and S2. A Pb shield with same geometry and dimensions as each PS is placed in front of them, with the plane containing the barycenter of the shield being identical to the one containing the interface between S1 and S2. Thermal neutron converters are modeled as two natural, 100-% pure Gd. This model is representative of 250-µm sheets commercialized by Goodfellow [16], and whose purity is certified as superior or equal to 99 %.

Californium-252 has a typical spontaneous-fission-type neutron emission spectrum [17]. This neutron spectrum is modeled with MCNP6.1 by means of a Watt distribution, which associates to every energy E_n of a fission neutron a value of the emission density of probability $f(E_n)$ as

$$f(E_n) = C \cdot \exp\left(-\frac{E_n}{a}\right) \cdot \sinh(\sqrt{bE_n}) \quad (1)$$

with parameters $(C; a; b) = (0.3016; 1.025\ \mathrm{MeV}; 2.926\ \mathrm{MeV^{-1}})$. Spontaneous fissions account for $\Gamma_f = 0{,}0309\ \mathrm{f.dis^{-1}}$ (fission per disintegration) of Cf-252. A sealed Cf-252 sample is a mixed n/γ source, with mean number of emitted neutrons per fission $\nu_n = 3.77\ \mathrm{n.f^{-1}}$, and mean number of emitted gamma rays per fission $\nu_\gamma = 7.98\ \gamma.\mathrm{f^{-1}}$ [18], as kept for this study. The gamma-ray spectrum accompanying spontaneous fissions is modeled as a piecewise density function [19]. The Cf-252 emitter is simulated under the form of an isotropic point source, in contact with the Pb shield and aligned with its center of mass.

Eight irradiation configurations were simulated, where the number of Gd sheets used (from 0 up to 2) and their disposition are varied in the setup. Configurations are indexed from 1 to 8, with description in Table I. These series have been defined to highlight the increase in total response ($\mathrm{d.dis^{-1}}$) brought by the inversion of Gd. The front face of one PS is the one in contact

with Pb, the back face as the one parallel to the front face and farther from the source. Fig. 1a) represents the model of the test bench (Moritz1.23 software was used for visualization [20]).

Neutron and gamma-ray emissions are simulated separately. The macroscopic estimate of the energy laid down by incident gamma rays in S1 and S2 is delivered by tally 8 of MCNP.1: it is labeled $\tau_\gamma(E_\gamma)$, and expressed in gamma-ray energy depositions per generated gamma ray and per energy bin. The PS response to the neutron emission of Cf-252 has two components:

- the energy laid down by gamma rays released after radiative capture of moderated neutrons. In series 2 to 8, where Gd converters are added to the sensor, this contribution is filled by the de-excitation source term provided by the MCPN6.1 code-backed, ENDF/B-VII.1 library [21]. The selection of this library was justified by a verification of the faithful estimation of the freed energy [22]. Moreover, in all configuration, S1 and S2 have intrinsic gamma-ray response to moderated neutrons, mainly through $^{1}\mathrm{H}(\mathrm{n},\gamma)$ and $^{12}\mathrm{C}(\mathrm{n},\gamma)$ capture reactions [23]. Prompt gamma rays from these captures are also generated with ENDF/B-VII.0. The sum of all (n,γ) contributions, provided by tally 8, is labeled $\tau_{(n,\gamma)}(E_\gamma)$ and expressed in gamma-ray energy depositions per generated neutron and per energy bin;
- the energy laid down by recoil nuclei along the diffusion of incident neutrons. Given the 1000-cm^3 volume of both PS, and the neutron emission spectrum (mean energy around 2.3 MeV), its evaluation may be narrowed down to $^{1}\mathrm{H}(\mathrm{n},\mathrm{n})$ diffusions in plastic [24]. This contribution is delivered by tally 8 used with tally 6 and PHL option of MCNP6.1. It is labeled $\tau_{(n,n)}(E_p)$ and expressed in proton energy depositions per generated neutron and per energy bin.

TABLE I. DESCRIPTION OF THE EIGHT SIMULATED CONFIGURATIONS OF IRRADIATION

Series index	Description
1	No Gd sheet
2	1 Gd sheet (250 µm) between S1 et S2
3	2 Gd sheets (500 µm) between S1 et S2
4	1 Gd sheet on the front face of S1
5	1 Gd sheet on the front face of S2
6	1 Gd sheet on the front face of S1 1 Gd sheet on the back face of S2
7	1 Gd sheet on the front face of S1 1 Gd sheet on the front face of S2
8	1 Gd sheet on the back face of S1 1 Gd sheet on the front face of S2

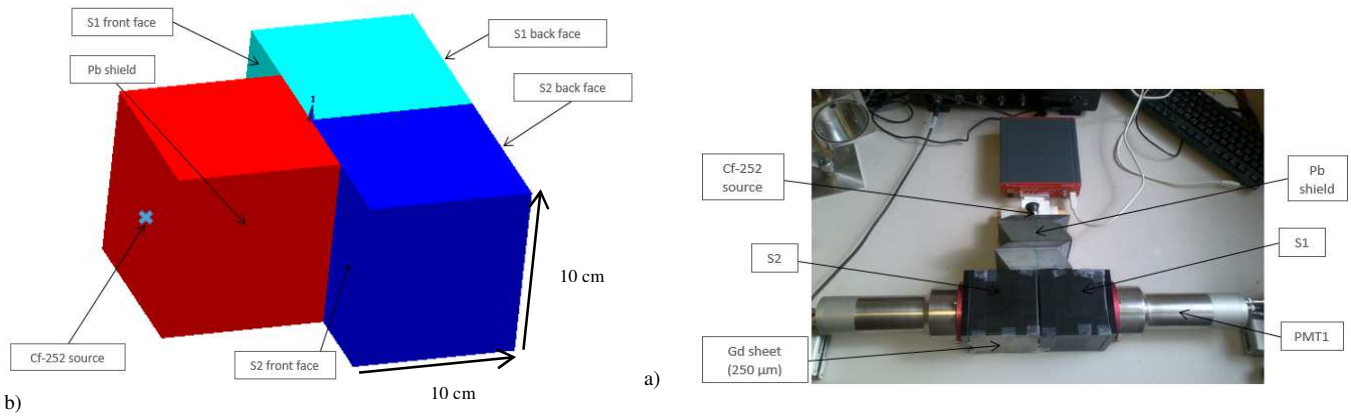

Fig. 1a) 3D-Representation of the bench model under MCNP6.1 (Moritz 1.23), and b) Experimental test bench (CEA LIST).

As we aimed at estimating the expected response at the output of a detection chain, it was necessary to convert every deposited energy E_γ or E_p (MeV) into the photoelectron response of the scintillation detectors, labeled E_{ee} and expressed in MeVee. This conversion depends on fluorescence quenching for recoil protons and secondary electrons, and is taken into account using the calibration by Pozzi *et al.* [25]. The expected spectral deposition rate per disintegration and per energy bin $Y(E_{ee})$ is ultimately derived as

$$Y(E_{ee}) = Y_\gamma(E_{ee}) + Y_{(n,\gamma)}(E_{ee}) + Y_{(n,n')}(E_{ee}) = \tau_\gamma(E_{ee}) \cdot \nu_\gamma \cdot \Gamma_f + \left(\tau_{(n,\gamma)}(E_{ee}) + \tau_{(n,n)}(E_{ee})\right) \cdot \nu_n \cdot \Gamma_f \quad (2)$$

Figures 2a) and b) below present the estimated $\tau_{(n,\gamma)}(E_{ee})$ (F8_p) and $\tau_{(n,n)}(E_{ee})$ (F8_h) responses for S1 in configurations 1 (no Gd) and 3 (500 µm of Gd). The comparison between both figures shows, according to Part II, a significant increase in the high-energy (> 3 MeVee) component of $\tau_{(n,\gamma)}$ from series 1 to 3, attributable to $\mathrm{Gd(n,\gamma)}$ captures. This interpretation is corroborated by the spectral evolution of photon fluence $\psi_{(n,\gamma)}(E_{ee})$ in S1, expressed in photon per generated neutron and centimeter square ($\mathrm{ph.n^{-1}.cm^{-2}}$), and estimated by means of tally 4. Rays at 2.22 MeVee from $^{1}\mathrm{H(n,\gamma)}$ and 4.95 MeVee from $^{12}\mathrm{C(n,\gamma)}$ are clearly identified on both figures. Fluence $\psi_{(n,\gamma)}(E_{ee})$ associated with series 3 additionally reveals a continuum up to the Q-values of $^{157}\mathrm{Gd(n,\gamma)}$ (7.9 MeVee) and $^{155}\mathrm{Gd(n,\gamma)}$ (8.5 MeVee) reactions. Thus the input of Gd in the high-energy response of the detector is qualitatively established.

In view of a quantitative review of simulation results, the full spectral response $Y(E_{ee})$ for all eight configurations is integrated between a varying lower bound $s \in \{2; 2.5; 3; 4\}$ MeVee and an upper bound set equal to 9 MeVee. The integrated response $Y(s)$ is expressed in $\mathrm{d.dis^{-1}}$. Figures 3a) and 3b) illustrate the evolution of Y as a function of series index from Table I, for $s = 2.5$ MeVee and $s = 3$ MeVee in S1. All configurations in which a Gd converter is added to the sensor have higher Y response than series 1, whatever the value of s. The highest expected increase is noted for series 2 and 3, where Gd is inserted between S1 and S2, and is more drastic as s increases: from series 1 to series 3 in S1, for instance, Y is multiplied by a factor 2.5 for $s = 2$ MeVee, 4 for $s = 2.5$ MeVee and $s = 3$ MeVee, and 7 for $s = 4$ MeVee.

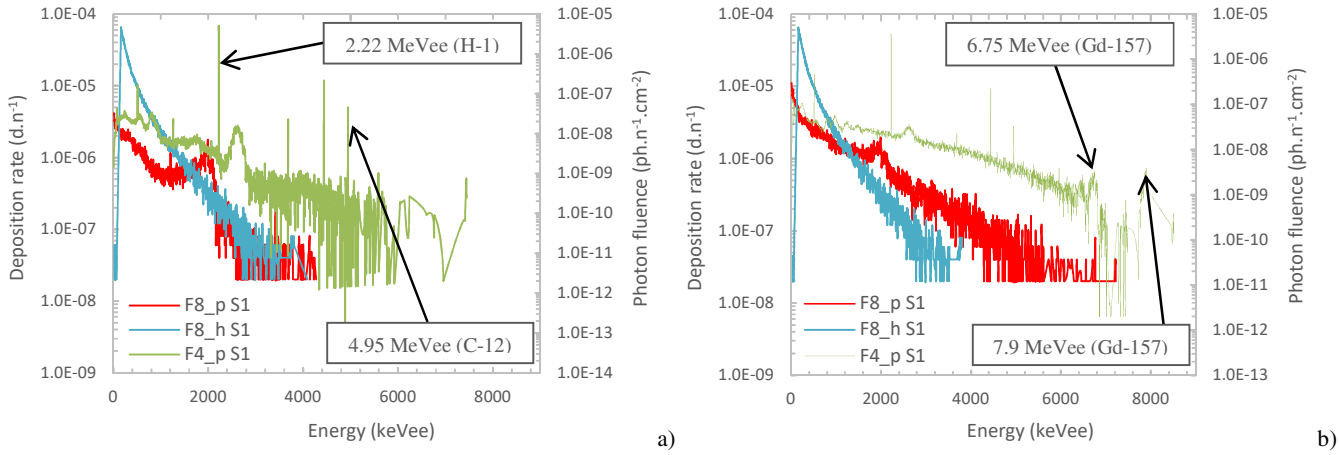

Fig. 2. Macroscopic estimates from MCNP6.1 for a) series 1, and b) series 3.

B. *Test bench and experimental response to a shielded Cf-252 source*

To investigate the modeling scheme presented in paragraph III.A, we reproduced experimentally the irradiation conditions detailed above and illustrated in Fig. 1a). The test bench, depicted in Fig. 1b), has two EJ-200 and two photomultipliers tubes (PMT) mounted by pairs and isolated from ambient light. PMT are polarized between -1500 V (channel S1) and -1535 V (S2). The acquisition chain samples the signal with the frequency of 200 MS.s^{-1} on both channels. A calibration coefficient equal to 76 keVee.channel^{-1} was estimated with Co-60, so that the trigger set at channel 7 corresponds to a 531-keVee counting threshold.

Net count rate spectra, labeled $\lambda(E_{ee})$ and expressed in count per second and per energy bin, are acquired for experimental configurations 1 to 8 from Table I. The high-energy background count rate from gamma-ray activity and cosmic muons, integrated between a lower bound s and an upper bound of 9 MeVee, was found to range from $\lambda(s = 4\ \mathrm{MeVee}) = 3.11 \pm 0.06$ cps to $\lambda(s = 2\ \mathrm{MeVee}) = 5.80 \pm 0.08$ cps.

The mixed emitter was a sealed Cf-252 source of activity $A = 580 \pm 87$ kBq. Count rate is divided by A to form a spectral distribution $R(E_{ee})$, expressed in count per disintegration and per energy bin, which is homogenous to the estimated $Y(E_{ee})$ from paragraph III.A. The experimental spectral response $R(E_{ee})$ is integrated between $s \in \{2; 2.5; 3; 4\}$ MeVee and 9 MeVee. The integrated response $R(s)$ is expressed in count per disintegration of Cf-252 ($\mathrm{c.dis^{-1}}$). Figures 3a) and 3b) illustrate the evolution of R, superimposed to Y, as a function of series index from Table I, for $s = 2.5$ MeVee and $s = 3$ MeVee in S1. Error bars correspond to one standard deviation in Poisson counting statistics.

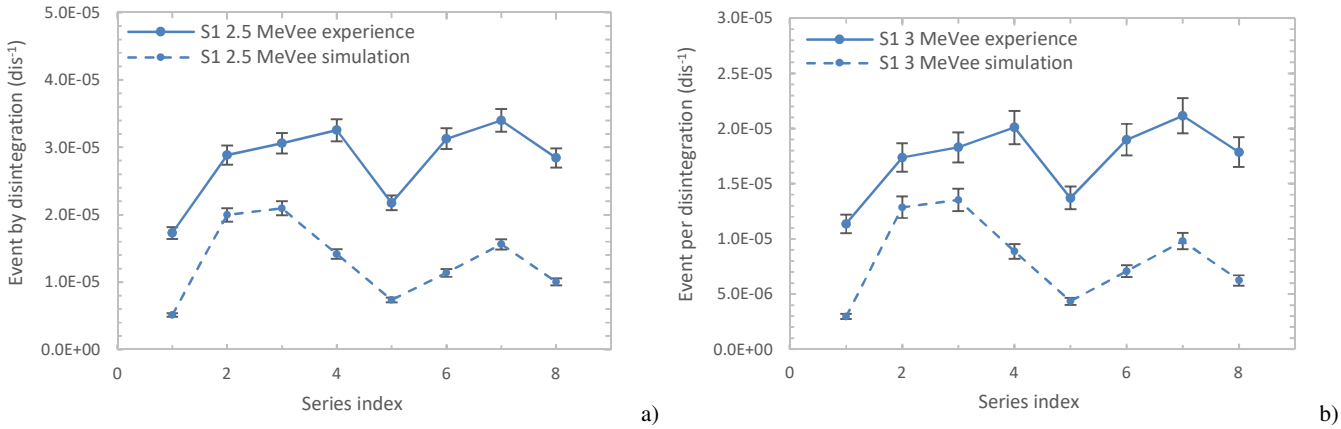

Fig. 3. Experimental R and simulated Y responses of S1 as a function of series index for a) $s = 2.5$ MeVee, and b) $s = 3$ MeVee.

C. *Comparative study and first conclusions*

Comparison between Y and R shows similar trends as series indices are screened, for all threshold values s and both PS. We can noticeably verify that the lowest response R always corresponds to configuration 1 (no Gd), in agreement with simulations. The highest experimental increase is noted for series 2, 3, 6 and 7, and lies around a factor of 2 for all considered values of s. The relative increase of high-energy signal, obtained by insertion of Gd converters, is therefore in the order of our expectations, although by lesser values. This tends to indicate that the relative contribution of (n,γ) to the total response is lower in our experiments than in the idealized model of paragraph III.A.

We thus confirmed experimentally the relative evolution of Y as the Gd-insertion configuration varies, while highlighting discrepancies that need to be discussed. As the numerical code presented in paragraph III.A is to serve the conception of a PHD discrimination scheme in a composite PS/Gd sensor, we still have to investigate the absolute agreement of responses Y and R, at least as far as orders of magnitude are concerned. The most interesting series for the rest of the study are configurations 2 and 3, in which a 250 to 500-µm layer is inserted between S1 and S2. Now, over S1 and S2, relative differences between R and Y lie between 47 and 49 % for $s = 2$ MeVee, 45 and 46 % for $s = 2{,}5$ MeVee, and around 35 % for $s = 3$ MeVee. Relative differences over other series are found below 100 % for $s = 2$ MeVee, and below 200 % for $s = 2.5$ MeVee to $s = 4$ MeVee.

Given the number and the variety of contributions to the high-energy response we listed in paragraph III.A, an experimental corroboration of the expected order of magnitude is a satisfactory result, and confirms the usability of the modelling scheme as a scaling tool for an optimized material design. The comparative study shows, however, that the measured total signal is systematically higher than the expected response, while relative trends appear consistent with numerical estimated. This may be imputed to several factors that non-mutually exclusive:

- simulations do not account for neutron and gamma-ray room return in the environment of the measurement bench, that only tends to increase the number of interaction events in the detection ensemble;
- while simulations describe as finely as possible the material bricks used in experiment, dimension (in the order of 1 mm) and position (in the order of 1 cm) uncertainties are admitted. The same statement is true as far the composition and structure (for PS) of interaction media, not to mention the 15-% one standard-deviation attached to Cf-252 source activity;
- fluorescence quenching afflicting the measured energy from proton recoils may be underestimated, as the phenomenon is scarcely described in literature ;
- limits exist regarding de-excitations models for Gd-156* and Gd-158* nuclei [26,27], as already mentioned in Section II.

The following sections will be devoted to the coupling of this model of PHD to the implantation of multiplicity-based temporal filtering.

IV. Building and Pre-Validation of a Numerical Code for the Study of Gamma-Ray Coincidence Filtering

Gamma-ray events in S1 and S2 may be due to background radiation and as well as neutron capture in the matrix and in Gd converters. However, due the emission multiplicity in $\mathrm{Gd}(\mathrm{n},\gamma)$ captures, and provided that the Gd-converter is inserted between adjacent PS, there is a probability that at least one photon will interact in S1 and one photon will interact in S2. In such a scenario, illustrated in Fig. 4a), neutron capture will be followed by two quasi-coincident energy depositions on a both channels. By designing a *γ-γ coincidence filtering* algorithmic architecture, we may thus expect a drastic reduction of high-energy gamma vulnerability and an increase in n/γ discrimination ratio, at the expense, however, of neutron sensitivity. To quantify numerically the impact of such a filtering, we needed to the complete history of every primary and secondary particle inside the detection ensemble.

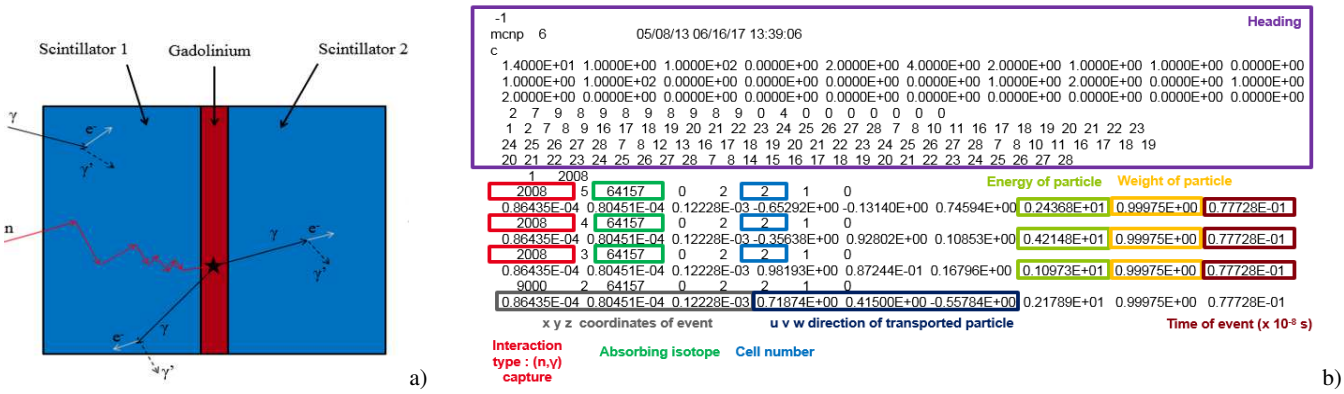

Fig. 4a) Side-view of a multiple-gamma emission following $\mathrm{Gd(n,\gamma)}$ capture, and b) MCNP6.1 Particle TRAck file associated with such event.

A. *Post-treatment code of MCNP.1 Particle TRAck files for the study of filtering*

MCNP6.1 tallies 4, 6 and 8 only provide macroscopic estimates of a physical quantity (flux, reponse) computed over a large number of random draws. To study the influence on such quantities of a multiplicity-based filtering, it was necessary to analyze the content of said Particle TRAck files that store, for a simulated data set, all information related to a selected particle type, either produced or interacting according to a specified mode. Figure 4b) reproduces the content of such a file associated a gamma-ray emission with a multiplicity of 3, following $^{157}\mathrm{Gd(n,\gamma)}$ capture inside the converter. It is notably possible to identify the type of interaction undergone by the particle, the number of the cell in which the interaction took place, the involved isotope, and the energy of the particle before and after interaction.

A numerical code was thus developed in order to automatically reconstruct the expected filtered spectral neutron responses $Y_{\mathrm{filt}}(E_{ee})$ on the basis of: joint energy deposition in S1 and S2, above a given energy threshold (hereby set equal to 531 keVee) and associated with the same photon creation event, either unique or multiple. Event-by-event post-treatment and reconstruction of filtered spectra are coded in Matlab® [28] environment, following the functional flow chart draw represented in Fig. 5a). Energies E_{ee} (in MeVee) laid down in S1 and S2, for every gamma-ray creation history, are thus stored in a response histogram with, on the *y*-axis, the number $\tau(E_{ee})$ of deposition per generated neutron and per energy bin. If we label $E_{ee1,i}$ and $E_{ee2,i}$ the energies laid down in S1 and S2 respectively, for a given history i, then the pseudocode translation of the coincidence gate that produces the filtered response $\tau_{\mathrm{filt}}(E_{ee})$ should read

$$\begin{gathered}\text{IF } (E_{ee1,i} > 531 \text{ keVee AND } E_{ee2,i} > 531 \text{ keVee})\\ \text{THEN } E_{ee1,i} = E_{ee1,i} \text{ and } E_{ee2,i} = E_{ee2,i}\\ \text{ELSE } E_{ee1,i} = 0 \text{ and } E_{ee2,i} = 0\end{gathered}$$

We note that, if the filtering function is removed from the flow chart, the reconstructed spectral response should be identical to tally 8 of MCNP6.1. We used this fact to pre-validate numerically our simulation scheme, as detailed in next paragraph.

B. *Comparison of energy depositions rates from MCNP6.1 tallies and post-treatment of Particle TRAck files*

The adequacy of the reconstruction code was pre-validated by comparing the outputs obtained from the implementation of flow chart in Fig. 5a) (without multiplicity filtering) and the macroscopic response provided by tally 8 of MCNP6.1. Using notations from paragraph III.A, we limit the study to deposition rates $\tau_{\gamma}(E_{ee})$ and $\tau_{(n,\gamma)}(E_{ee})$, depending on the nature of the primary radiation source. Spectral deposition rates are labeled $\tau_{MCNP}(E_{ee})$ when obtained from tally 8 and $\tau_{PTRAC}(E_{ee})$ when produced by post-treatment of Particle Track files. This simulation study is carried out with material disposition corresponding to configuration 2 from Table I, and rates are compared over S1.

Four radiation sources are simulated, two of them related to gamma-ray emission, and two of them representative of neutron emission, with increasing complexity:

- Test 1: Single-energy (662 keV) homogenous emission in the central Gd converter;
- Test 2: Gamma-ray emission spectrum of Cf-252 from a point-source against the detection ensemble;
- Test 3: Homogenous thermal neutron (25 meV) emission inside Gd;
- Test 4: Neutron emission spectrum of Cf-252 from a point-source against the detection ensemble.

The agreement between $\tau_{MCNP}(E_{ee})$ and $\tau_{PTRAC}(E_{ee})$ is illustrated in Fig. 5b) below in the case of Test 3.

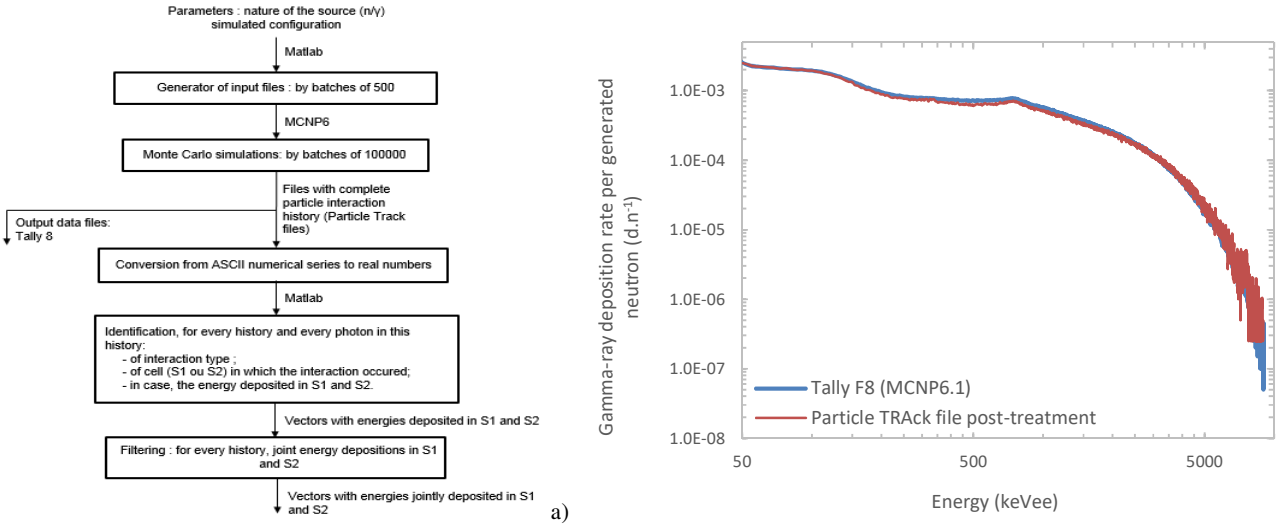

Fig. 5a) Flow chart of Particle Track file post-treatment, and b) Spectral rates $\tau_{MCNP}(E_{ee})$ and $\tau_{TRAC}(E_{ee})$ for Test 3.

The quantitative comparison of outputs is based on the relative difference $\varepsilon_{\%}(s)$ between spectral rates integrated from a varying lower bound $s \in \{50; 531; 2000\}$ keVee to an upper bound equal to 9 MeVee:

$$\varepsilon_{\%}(s) = 100\ \% \cdot \frac{\tau_{PTRAC}(s) - \tau_{MCNP}(s)}{\tau_{MCNP}(s)} = 100\ \% \cdot \frac{\int_s^{9\ \mathrm{MeVee}} \tau_{PTRAC}(E_{ee})dE_{ee} - \int_s^{9\ \mathrm{MeVee}} \tau_{MCNP}(E_{ee})dE_{ee}}{\int_s^{9\ \mathrm{MeVee}} \tau_{MCNP}(E_{ee})dE_{ee}} \quad (3)$$

Values of $\varepsilon_{\%}(s)$ are presented in Table II, and range from 1 to 15 % in absolute. This confirms the accurate reconstruction of unfiltered gamma-ray deposition rates from gamma-ray and neutron sources by means of the numerical post-treatment code developed for this study. We therefore transposed the implementation of the said code to the simulation of expected filtered response Y_{filt}, in c. dis^{-1}, to a Pb-shielded Cf-252 source.

TABLE II. RELATIVE DIFFERENCES BETWEEN INTEGRATED OUTPUTS $\tau_{MCNP}(s)$ ET $\tau_{TRAC}(s)$

Test label \ Integration threshold s	50 keVee	531 keVee	2 MeVee
Test 1	- 2.9 %	- 11.1 %	-
Test 2	- 2.2 %	- 2.4 %	14.7 %
Test 3	- 6.3 %	- 6.2 %	1.2 %
Test 4	- 6.2 %	- 9.0 %	- 1.3 %

C. *Estimates of signal evolution in a multiplicity-based gamma-ray event filtering*

The entire algorithmic sequence illustrated in Fig. 5a) was implemented in Particle TRAck file post-treatment. To highlight the benefit from Gd in multiplicity-based detection scheme, we computed the expected filtered spectral response $Y_{\mathrm{filt}}(E_{ee})$ in configurations 1 (no Gd) and 2 (250-µm converter between S1 and S2) from Table I. As in paragraph III.A, responses gamma-ray and neutron emissions of Cf-252 are obtained separately, and averaged to one disintegration of the radionuclide using Eq. (2). The Pb shield used in experiments is modeled, and the position of the source is identical to the one considered in paragraph III.A.

The multiplicity-filter described in paragraph IV.A is an ideal γ-γ coincidence filter. It follows that $Y_{(n,n'),\mathrm{filt}}(E_{ee}) = 0$ by construction. In simulated configuration, contribution from $Y_{\gamma,\mathrm{filt}}(E_{ee})$ are also negligible. The comparison between unfiltered $Y(E_{ee})$ and filtered $Y_{\mathrm{filt}}(E_{ee})$ spectral responses thus essentially informs us on the reduction of post-filtering neutron signal $Y_{n,\mathrm{filt}}(E_{ee})$. Integrated responses $Y(s)$ et $Y_{\mathrm{filt}}(s)$, between $s = 531$ keVee and 9 MeVee, and expressed in energy deposition per disintegration of Cf-252 (d.dis^{-1}), are presented in Table III below.

TABLE III. SIMULATED (IN D.DIS^{-1}) AND EXPERIMENTAL (IN C.DIS^{-1}) RESPONSES INTEGRATED FROM 531 KEVEE

Series index \ Response	Y(531 keVee)	Y_{filt}(531 keVee)	R(531 keVee)	R_{filt}(531 keVee)
Series 1	$(3.05 \pm 0.03)\cdot 10^{-4}$	$(5.13 \pm 0.77)\cdot 10^{-6}$	$(3.00 \pm 0.03)\cdot 10^{-4}$	$(1.7 \pm 0.2)\cdot 10^{-6}$

Series 2	$(4.20 \pm 0.04)\cdot 10^{-4}$	$(2.75 \pm 0.41)\cdot 10^{-5}$	$(3.57 \pm 0.03)\cdot 10^{-4}$	$(3.3 \pm 0.3)\cdot 10^{-5}$

Two major conclusions may be drawn from the simulation-based estimates consigned in Table III:

- Comparing Y_{filt} from series 1 to series 2, the adding of a central Gd layer leads to an increase of neutron response by a factor of 60. It thus appears necessary to use multiple-gamma-ray-emitter Gd nuclei after neutron capture to consolidate the detection scheme *via* a γ-γ coincidence filtering method;
- In presence of a 250-µm Gd converter (series 2), the filtered neutron response Y_{filt} is found reduced by a factor of 15 when compared to the unfiltered response Y.

We then estimated a neutron sensitivity reduction by approximately one order of magnitude in an ideal γ-γ coincidence filtering. The benefit of such a discrimination scheme as far as gamma-ray vulnerability and detection limits will be studied experimentally in the following section.

V. Experimental study of N/Γ discrimination by quasi-coincidence filtering

An experimental study reproducing the irradiation configurations 1 and 2 described in Section IV was conducted in order to verify the one-order-of-magnitude neutron signal reduction and the impact on background-induced false counting *via* a multiplicity-based event discrimination. Given the sampling frequency of 200 MS.s^{-1} of the pulse acquisition chain, the n/γ discrimination scheme was implemented as a quasi-coincidence-gated filter with a temporal window of 5 ns between channels 1 and 2. Pulse processing returns a filtered count rate $\lambda_{\text{filt}}(s)$ (in c.s^{-1}) integrated between the trigger threshold $s = 531$ keVee on both channels and the upper threshold of 9 MeVee. The test bench is otherwise identical to the one described in paragraph III.B and depicted in Fig. 1b).

A. *Experimental results and comparison with simulations*

We considered irradiation configurations 1 and 2 of Table I, with the same Pb-shielded Cf-252 source as used in paragraph III.B. For the sake of investigating of the merits of quasi-coincidence filtering, both filtered $\lambda_{\text{filt}}(s)$ and unfiltered $\lambda(s)$ count rates were averaged to one disintegration of radionuclide using the activity of the source. The obtained experimental responses $R(s)$ (no filtering) and $R_{\text{filt}}(s)$ (5-ns quasi-coincidence filtering), in c.dis^{-1}, are presented in Table III supra to allow a quantitative comparison with simulation outputs.

Responses Y and R stand in in good absolute agreement, with relative differences between experience and simulation about 1.7 % for series 1 and 18 % for series 2, which goes to the validation of the PHD modeling scheme argued in paragraph III.C. Filtered responses Y_{filt} and R_{filt} are also found compatible, with -17 % relative difference between experience and simulation for series 2, and same order of magnitude over series 1. Furthermore, both key conclusions from paragraph IV.C are experimentally corroborated. First, we verified the insertion of a Gd-converter has a drastic impact on detection with a quasi-coincidence filter, R_{filt} being multiplied by a factor of 20 from series 1 to series 2 (against 60 in simulations). Second, as far as series 2 is concerned, the ratio $\frac{R}{R_{\text{filt}}} = 9$ confirms the one-order-of magnitude reduction of neutron response when implementing a quasi-coincidence filtering method (to be compared with $\frac{Y}{Y_{\text{filt}}} = 15$ in simulations).

The next point of the experimental study regards the impact of quasi-coincidence filtering on gamma- and cosmic-ray background reduction. We selected configuration 2 from Table I for this assessment. First acquisitions were carried out in the absence of radiation source, the dose rate at the detector level being then measured as equal to 75 nSv.h^{-1} with a commercial Thermo Electron ESM FH 40G-L 10 radiameter. Integrated count rates between 531 keVee and 9 MeVee read as $\lambda(531\,\text{keVee}) = 35{,}9 \pm 0{,}2\,\text{c.s}^{-1}$ without filter and $\lambda_{\text{filt}}(531\,\text{keVee}) = 0$ with quasi-coincidence filter. Next acquisitions were performed in presence of an unshielded Na-22 source in front of the Gd/PS detection ensemble, inducing a 14-µSv.h^{-1}-dose rate at the detector level. Integrated unfiltered and filtered count rates then read as $\lambda(531\,\text{keVee}) = 7989{,}5 \pm 40{,}0\,\text{c.s}^{-1}$ and $\lambda_{\text{filt}}(531\,\text{keVee}) = 3 \pm 0{,}8\,\text{c.s}^{-1}$. Therefore, cancellation of natural background and reduction of Na-22 background rate by a factor of 2700 were observed with the implementation of the filter, emphasizing the consolidation of the algorithmic architecture with regards to background radiations.

B. *Estimates of figures of merits*

The general agreement between simulated and experimental responses from Table III allows us, in first approach, to discuss the values of R_{filt} in light of the conclusions drawn in the end of Section IV.

Observations from paragraph IV.B highlight that filtered response Y_{filt}, and therefore its consistent counterpart R_{filt}, may be identified to the detector response to the sole neutron component of Cf-252 emission. We may thus deduce from R_{filt} a first estimate of neutron sensitivity, labeled $\widehat{S_n}(s)$, of the multiplicity-based counting scheme (hereby the detection threshold $s = 531$ keVee on channels 1 and 2). Neutron dose rate at the detector level is measured as $\Delta_n = 10\,\mu\text{Sv.h}^{-1}$ by means of a calibrated, commercial neutron probe reference LB 6411 (BERTHOLD FRANCE SAS). Using Cf-252 source activity A, the neutron sensitivity estimated in configuration 2 reads a

$$\widehat{S_n}(531\,\text{keVee}) = \frac{R_{\text{filt}}(531\,\text{keVee}) \cdot A}{\Delta_n} \sim 7\,\text{c.nSv}^{-1} \quad (4)$$

The obtained estimate is quite high, in the 1-c.nSv^{-1} order of magnitude of commercial, He-3 proportional counter sensitivity [29].

We recall that this estimate of $\widehat{S_n}$ is based on the assumption that gamma-ray contribution from Cf-525 to $R_{\text{filt}}(531\text{ keVee})$ is negligible. Let alone the absolute agreement between $Y_{\text{filt}}(531\text{ keVee})$ and $R_{\text{filt}}(531\text{ keVee})$, this assumption is backed by the measurement of Cf-252-induced gamma-ray dose rate at the detector level in configuration 2, found equal to $\Delta_\gamma = 2\ \mu\text{Sv.h}^{-1}$. Now, using the Na-22 measurement described at the end of paragraph V.A, it is possible to estimate the neutron detection scheme vulnerability to a high-energy (1274.5 keV) gamma-ray background, labeled $\widehat{V_\gamma}(s)$, as

$$\widehat{V_\gamma}(531\text{ keVee}) = \frac{\lambda_{\text{filt},\gamma}(531\text{ keVee})}{\Delta_\gamma} \sim 0.8\text{ c.nSv}^{-1} \quad (5)$$

Using this estimate, we may derive an expected contribution from Cf-252 gamma-ray background to experimental response in configuration 2: $\widehat{R_{\text{filt},\gamma}}(531\text{ keVee}) = 7 \cdot 10^{-7}\text{ c.dis}^{-1}$, hence a relative contribution from false neutron counting

$$\frac{\widehat{R_{\text{filt},\gamma}}(531\text{ keVee})}{R_{\text{filt}}(531\text{ keVee})} = \frac{7 \cdot 10^{-7}}{3{,}3 \cdot 10^{-5}} \sim 2\ \% \quad (6)$$

which is indeed negligible. The main bias attached to this verification lies within the wide spectral extent of prompt gamma-ray emission from Cf-252, notably above 1.5 MeV. Now penetrating power increases with gamma-ray energy, meaning that for the same dose rate, a higher-energy source would be likely to induce a superior true quasi-coincident response, and therefore higher gamma-ray vulnerability $\widehat{V_\gamma}$. This point is however to be tempered by the fact that mean energy of Cf-252 prompt gamma-ray [30] is calculated as $\overline{E_\gamma} = 875$ keV, and consequently far below to the energy of Na-22 prominent gamma-ray line. The evolution of figure $\widehat{V_\gamma}$, for a given dose rate, a function of gamma-ray energy of emission, will be studied in future word, notably as far as higher-energy emitters, such as Th-232, are involved.

Experimental quasi-coincidence filtered response over S1 and S2, above a PHD threshold set equal to 531 keVee, led to a one-order-of-magnitude loss in neutron sensitivity, and a 1700-factor of gamma-ray background count rate when compared to unfiltered response above the same PHD threshold. Estimates of neutron detection limit, labeled $\widehat{DL_n}$ and expressed in neutron per centimeter square and per second ($\text{n.cm}^{-2}.\text{s}^{-1}$), are conventionally [31] derived as a function of acquisition time t and gamma-ray dose rate Δ_γ

$$\widehat{DL_{\text{filt},n}}(\Delta_\gamma, t) = \frac{2{,}71 + 4{,}61\sqrt{\widehat{\lambda_{\text{filt},\gamma}}(\Delta_\gamma) \cdot t}}{\widehat{S_n} \cdot t} \quad (7)$$

From Eq. (7), it follows that quasi-coincidence filtering leads a lowering of detection limit by a factor of 5 from the unfiltered scheme in configuration 2, with implemented temporal gate and integration thresholds. From the prospective of n/γ discrimination ratio, estimated rates result in SNR around 150, which is close to the rejection ratio of 145 reported by De Vita *et al*. [8], in the frame of another multiplicity-based discrimination architecture.

The estimates of key factors of merit attached to the assessed, material and algorithmic architectures are summarized in Table IV.

TABLE IV. SETUP CHARACTERISTICS AND ESTIMATES OF KEY FIGURES OF MERIT

Material architecture	**Algorithmic architecture**	**Neutron sensitivity estimate**	**Gamma-ray background vulnerability**	**n/γ discrimination ratio estimate**
Two PS EJ-200 10 ×10 ×10 cm^3 250-µm Gd-nat between S1 et S2	Energy threshold: 531 keVee Quasi-coincidence filtering over S1 et S2 (Δt = 5 ns)	7 c.nSv^{-1} (Cf-252)	0.8 c.nSv^{-1} (Na-22, 14 µSv.h^{-1})	150 (Cf-252/Na-22)

VI. CONCLUSION

A numerical model of the material bricks forming the detection ensemble (PS, Gd, shields), as well as of two n/γ discrimination algorithmic architectures, was developed by means of the MCNP6.1. The post-treatment of output data allowed us to reconstruct the total spectral responses of both PS, as well as the responses associated with γ-γ coincidence filtering of multiple-gamma-ray events following $\text{Gd}(\text{n},\gamma)$ captures (Particle TRAck files). A complete test bench, and an electronic chain

dedicated to pulse acquisition and treatment was used to calibrate our numerical models of detection schemes, to interpretate relative trends and absolute orders-of-magnitude of neutron responses.

While neutron sensitivity was estimated close to $10\ \mathrm{c.nSv^{-1}}$, thus matching the gold standard of He-3 proportional counters, we derived, for our first setup and quasi-coincidence scheme, a gamma-ray vulnerability around $1\ \mathrm{c.nSv^{-1}}$. It follows that the estimated n/γ discrimination ratio of 150 was found inferior, by one order-of-magnitude, to the 10^3-figure of merit of He-3 counters. Furthermore, the latter ratio is consolidated up to 1-mSv.h^{-1} whereas the experiments described in this paper were limited to a 14-µSv.h^{-1} gamma-ray dose rate, *i.e.* almost two orders of magnitude below. In order to consolidate further the discrimination scheme, we will study, both by simulation and experimentally, the sensitivity and vulnerability of the PS/Gd ensemble when conserving quasi-coincidence filtering (5-ns gate), but elevating the PHD threshold on channels 1 and 2 above 500 keVee. Moreover, the experimental validation of numerical models, both in the case of standard and expert use of MCNP6.1 output files, will allow us to extract rules for an optimized material design, closer to the ideal spherical geometry introduced in previous work

Eventually, alternative approaches such as a gamma-proton temporal correlation, within a 10 to 100-µs gate, and their articulation with γ-γ coincidence, will be investigated in future work.

ACKNOWLEDGEMENTS

The authors thank CEA DAM, France, for funding this research.

REFERENCES

[1] R. Coulon, J. Dumazert, F. Carrel, M. Hamel, "Détecteur de neutrons, à plastique scintillant, entourant un cœur de gadolinium ou de cadmium, et couverture scintillante dopée ou couverte par du bore ou du lithium, et dispositif de comptage de neutrons associé", Commissariat à l'Energie Atomique, Patent Application WO2017191133A1 (2017).

[2] J. Dumazert, R. Coulon, F. Carrel, G. Corre, S. Normand, L. Méchin, M. Hamel, "Sensitive and transportable gadolinium-core plastic scintillator sphere for neutron detection and counting", *Nuclear Instruments and Methods in Physics Research A*, Vol. 828, pp. 181-190 (2016).

[3] G. H. V. Bertrand, M. Hamel, S. Normand, F. Sguerra, "Pulse shape discrimination between (fast and thermal) neutron and gamma rays with plastic scintillators: State of the art", *Nuclear Instruments and Methods in Physics Research Section A*, Vol. 776, pp. 114-128 (2015).

[4] B. Pritychenko , E. Běták, M. A. Kellett, B. Singh, J. Totans, "The Nuclear Science References (NSR) database and Web Retrieval System", *Nuclear Instruments and Methods in Physics Research A*, Vol. 640, Iss. 1, pp. 213-218 (2011).

[5] Y. Sakurai, T. Kobayashi, "Experimental verification of the nuclear data of gadolinium for neutron capture therapy", *Journal of Nuclear Science and Technology*, Vol. 39, Sup. 2, pp. 1294-1297 (2002).

[6] M. E. Medhat, Y. Wang, "Estimation of background spectrum in a shielded HPGe detector using Monte Carlo simulations", *Applied Radiation and Isotopes*, Vol. 84, pp. 13-18 (2014).

[7] J. H. Hubbell, S. M. Seltzer, Tables of X-Ray Mass Attenuation Coefficients and Mass Energy-Absorption Coefficients from 1 keV to 20 MeV for Elements $Z = 1$ to 92 and 48 Additional Substances of Dosimetric Interest, Radiation Physics Division, PML, NIST (1996).

[8] R. De Vita, F. Ambi, M. Battaglieri, M. Osipenko, D. Piombo, G. Ricco, M. Ripani, M. Taiuti , "A large surface neutron and photon detector for civil security applications", *Nuclear Instruments and Methods in Physics Research A*, Vol. 617, Iss. 1-3, pp. 219-222 (2010).

[9] E. Fanchini, "Performance of an RPM Based on Gd-lined Plastic Scintillator for Neutron and Gamma Detection", *IEEE Transactions on Nuclear Science*, Vol. 33, Iss. 1, pp. 392-399 (2016).

[10] I. A. Pawełczak, J. Tõke, E. Henry, M. Quinlan, H. Singh, W. U. Schröder, "NSTAR – A capture gated plastic neutron detector", *Nuclear Instruments and Methods in Physics Research A*, Vol. 629, pp. 230-238 (2011).

[11] Y. Kuroda, S. Oguri, Y. Kato, R. Nakata, Y. Inoue, C. Ito, M. Minowa, "A mobile antineutrino detector with plastic scintillators", *Nuclear Instruments and Methods in Physics Research A*, Vol. 690, pp. 41-47 (2012).

[12] S. Oguri, Y. Kuroda, Y. Kato, R. Nakata, Y. Inoue, C. Ito, M. Minowa, "Reactor antineutrino monitoring with a plastic scintillator array as a new safeguard", *Nuclear Instruments and Methods in Physics Research A*, Vol. 757, pp. 33-39 (2014).

[13] C. Roecker, A. Bernstein, N. S. Bowden, B. Cabrera-Palmer, S. Dazeley, M. Gerling, P. Marleau, M. D. Sweany, K. Vetter, "Design of a transportable high efficiency fast neutron spectrometer", *Nuclear Instruments and Methods in Physics Research A*, Vol. 826, pp. 21-30 (2016).

[14] D. B. Pelowitz (Ed.), *MCNP6™ User's Manual Version 1.0*, Los Alamos National Laboratory report, LA-CP-13-00364, Rev. 0 (2013).

[15] www.eljentechnology.com/products/plastic-scintillators/ej-200-ej-204-ej-208-ej-212

[16] www.goodfellow.com/E/Gadolinium-Foil.html

[17] K. Anderson, J. Pilcher, H. Wu, *Neutron Irradiation Tests of an S-Link-over-G-Link System*, ATLAS Tile Calorimeter internal document (1999).

[18] T. E. Valentine, *Evaluation of Prompt Gamma Rays for Use in Simulating Nuclear Safeguard Measurements*, ORNL/TM/-1999/300, Oak Ridge National Laboratory, Oak Ridge, Tennessee (1999).

[19] R. B. Hayes, "Preliminary Benchmarking Efforts and MCNP Simulation Results for Homeland Security", *Nuclear Technology*, Vol. 168, N° 3, pp. 852-857 (2008).

[20] *Moritz Geometry Tool, Version 1.23, An Interactive Geometry Editor/Viewer for MCNP and MCNPX*, White Rock Science, Los Alamos, New Mexico (2012).

[21] M. B. Chadwick *et al.*, "ENDF/B-VII.1 Nuclear data for nuclear science and technology: cross sections, covariances, fission product yields and decay data", *Nuclear Data Sheets*, Vol. 112, Iss. 12, pp. 2887-2996 (2011).

[22] S. A. Enger, P. Munck af Rosenschöld, A. Rezaei, H. Lundqvist, "Monte Carlo calculations of thermal neutron capture in gadolinium: A comparison of GEANT4 and MCNP with measurements", *Medical Physics*, Vol. 33, N° 2, pp. 337-341 (2006).

[23] A. D. Carlson, V. G. Pronyaev, D. L. Smith, N. M. Larson, Z. Chen, G. M. Hale, F.-J. Hambsch, E. V. Gai, S.-Y. Oh, S. A. Badikov, T. Kawano, H. M. Hofmann, H. Vonach, S. Tagesen, "International Evaluation of Neutron Cross Section Standards", *Nuclear Data Sheets*, Vol. 110, Iss. 12, pp. 3215-3324 (2009).

[24] M. Marseguerra, E. Padovani, S. A. Pozzi, "Use of the MCNP-Polimi code for time-correlation safeguards measurements", *Progress in Nuclear Energy,* Vol. 43, N° 1-4, pp. 305-311 (2003).

[25] S. A. Pozzi, J. A. Mullens, J. T. Mihalczo, "Analysis of neutron and photon detection position for the calibration of plastic (BC-420) and liquid (BC-501) scintillators", *Nuclear Instruments and Methods in Physics Research A*, Vol. 524, pp. 92-101 (2004).

[26] Y. Chen, "Gadolinium neutron-capture gammas in Geant4", *AARM Workshop 2015*, Syracuse, Italia (2015).

[27] C. Roecker, "Geant4-Gd Shower Problem", *ANNIE Collaboration 10/27*, UC Berkeley, United States (2014).

[28] *MATLAB and Statistics Toolbox Release 2012b*, The MathWorks, Inc., Natick, Massachusetts, United States (2012).

[29] A. Klett, B. Burgkhardt, "The new remcounter LB 6411: Measurement of neutron ambient dose equivalent H*(10) according to ICRP60 with high sensitivity", *IEEE Transactions on Nuclear Science*, Vol. 44, N° 3, pp. 757-759 (1997).

[30] A. B. Smith, P. R. Fields, A. M. Friedman, "Prompt Gamma Rays Accompanying the Spontaneous Fission of Cf^{252}", *Physical Review*, Vol. 104, N° 3, pp. 699-702 (1956).

[31] G. R. Gilmore, *Practical Gamma-ray spectrometry*, 2nd Edition, John Wiley & Sons Ltd, The Atrium, Southern Gate, Chichester, West Sussex, England, pp. 117-118 (2008).